

Entanglement evaluation of non-Gaussian states generated by photon subtraction from squeezed states

Akira Kitagawa,^{1,2,*} Masahiro Takeoka,^{1,2} Masahide Sasaki,^{1,2} and Anthony Chefles³

¹*National Institute of Information and Communications Technology (NICT) 4-2-1 Nukui-Kita, Koganei, Tokyo 184-8795 Japan*

²*Core Research for Evolutional Science and Technology (CREST), Japan Science and Technology Agency
1-9-9 Yaesu, Chuoh, Tokyo 103-0028 Japan*

³*School of Mathematical Sciences, University College Dublin, Dublin 4, Ireland*

(Dated: May 22, 2019)

We consider the problem of evaluating entanglement of the non-Gaussian mixed states generated by photon subtraction from the entangled squeezed states. The entanglement measures we use are the negativity and the logarithmic negativity. They enjoy the unusual property of being computable with linear algebra package even for high-dimensional quantum systems. We numerically evaluate these measures for the non-Gaussian mixed states which are generated by photon subtraction with on/off photon detectors. The results are compared with the behaviors of the operational measures, i.e., the teleportation fidelity and the mutual information in the dense coding scheme. Those results are qualitatively consistent with each other, that is, whenever the enhancement is seen in terms of the operational measures, the negativity and the logarithmic negativity are also enhanced.

PACS numbers: 03.67.Mn, 03.67.Hk, 42.50.Dv

I. INTRODUCTION

Continuous variable (CV) quantum optical systems are well-established tools for both theoretical and experimental investigations of quantum information processing (QIP) [1, 2]. The essential resource, entanglement, can be realized with a *Gaussian* two-mode squeezed vacuum state. This state is relatively easy to work with theoretically and is also commonly produced in the laboratory. It has been successfully applied to implement various important protocols, such as the quantum teleportation [3, 4, 5, 6], quantum dense coding [7, 8, 9] and entanglement swapping [10, 11]. These successes are based on well-developed techniques of optical Gaussian operations. These consist of beam splitting, phase shifting, squeezing, displacement, and homodyne detection.

However, recent theoretical investigations have shown some limits on such operations. A prime example is the no-go theorem relating to the distillation of entanglement shared by distant parties using only Gaussian local operations and classical communication (LOCC) [12, 13, 14]. To go beyond this limit, one should use higher order nonlinear processes, such as the cubic-phase gate [15] or Kerr nonlinearity [16]. It is, however, difficult to implement these nonlinear processes with presently available materials, which do not have sufficient level of nonlinearity yet and suffer from losses. Alternatively, a more practical method has been developed, which uses nonlinear processes induced by photon counting on tapped-off beams from squeezed states [17, 18, 19]. When ideal photon number resolving detectors are used, the input Gaussian

state can be transformed into a non-Gaussian pure state with higher entanglement. In practice, however, such detectors are not yet suitable for practical use. The most reliable type of photodetector available at present is the on/off type photon detector based on avalanche photodiodes. Such devices can only distinguish the vacuum ('off') state from non-vacuum ('on') states. The latter events result in a non-Gaussian mixed state. Evaluating the entanglement degree of such a state is far from trivial.

Previously, the effect of distillable entanglement has been theoretically analysed based on the figures of merit of concrete protocols, such as the fidelity of teleportation [20], the degree of violation of Bell-type inequalities [21, 22, 23] and the mutual information of dense coding [24]. In fact, it was shown that the performance of every protocol were improved, implying that the entanglement of the non-Gaussian mixed state must be enhanced. However, these indirect evaluations were dependent upon some external parameters, which depend upon specific operations differing protocol by protocol, such as the type of input state for the teleportation fidelity, the choice of the measurement basis for the Bell-type inequality violation, and the signal power of modulation for the dense coding.

Quantifying the entanglement of the photon-subtracted squeezed state of our interest here, in a way which is independent of particular external parameters, is an important issue. However, to our knowledge, it has not been previously addressed. For a state $\hat{\rho}$, an entanglement measure $E(\hat{\rho})$ should satisfy the following criteria [25]: (i) E is the non-negative functional, (ii) E vanishes if the state $\hat{\rho}$ is separable and (iii) E should not increase *on average* under LOCC. In general, a quantity satisfying these criteria is known as an entanglement monotone. Many such quantities have been proposed,

*Electronic address: kitagawa@nict.go.jp

such as the entanglement of formation [26, 27], the entanglement cost [28], the distillable entanglement [26], and the relative entropy of entanglement [29]. It is, however, not easy to calculate these measures for generic mixed states. Recently, however, two entanglement measures which are much more amenable to evaluation have been proposed. These are the negativity and the logarithmic negativity [30]. These measures are based on the Peres criterion [31]. That is, they are defined in terms of the eigenvalues of the partially-transposed density operator. The most distinctive feature of these entanglement measures is that they are easily computable numerically with linear algebra packages. Furthermore, the logarithmic negativity is an additive functional, and it is an upper bound on the distillable entanglement E_D [30].

In addition to being an entanglement monotone, it was believed that an entanglement measure E should also be convex (downward convex), i.e. it should be non-increasing on average under the loss of classical information by mixing. Convexity is necessary for an entanglement measure to be bounded from above by the entanglement of formation E_F [32], although the logarithmic function is concave (upward convex). Recently, however, it has been shown by Plenio *et al.* that convexity is not directly related to the physical process of discarding *quantum* information, i.e. discarding subsystems such as local ancillas during LOCC operations [33, 34] and that the logarithmic negativity is indeed a full entanglement monotone [34]. In view of these considerations, it is interesting to evaluate the entanglement of photon-subtracted mixed state in terms of the (logarithmic) negativities, and to compare them with the performance of protocols quantified by the operational measures.

This paper is organized as follows: In Sec. II, we briefly summarize the measurement-induced non-Gaussian operation on the two-mode squeezed vacuum state and its mathematical description. In Sec. III, the negativity and the logarithmic negativity are briefly reviewed, and their monotonicity is discussed. In Sec. IV, our numerical methods for calculating the negativities of the photon-subtracted mixed state are presented. In Sec. V, we review the previous analyses of the entanglement of such states using protocol-specific figures of merit. Those results are compared with each other. The final section VI is devoted to the discussion and conclusion.

II. MEASUREMENT-INDUCED NON-GAUSSIAN OPERATION

The schematic of the measurement-induced non-Gaussian operation on the two-mode squeezed state is shown in Fig. 1. The primary sources are two identical, single-mode squeezed vacuum states,

$$|r\rangle_k = \hat{S}_k(r)|0\rangle_k, \quad (1)$$

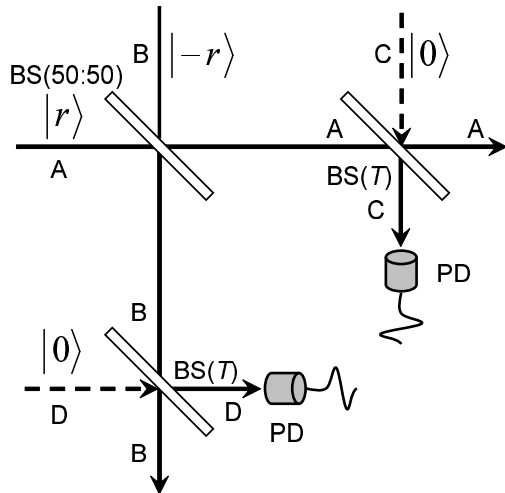


FIG. 1: Measurement-induced non-Gaussian operation on the two-mode squeezed vacuum state. BS, PS are beam splitter, photon detector, respectively.

where $\hat{S}_k(r)$ is the squeezing operator at path k ,

$$\hat{S}_k(r) = \exp \left[-\frac{r}{2} (\hat{a}_k^{\dagger 2} - \hat{a}_k^2) \right], \quad (2)$$

and r is the squeezing parameter. These are combined via a balanced beam splitter to generate the two-mode squeezed vacuum state,

$$\begin{aligned} |r^{(2)}\rangle_{AB} &= \hat{V}_{AB} \left(\frac{\pi}{4} \right) |r\rangle_A | -r\rangle_B \\ &= \hat{S}_{AB}(-r) |0\rangle_{AB} \\ &= \sum_{n=0}^{\infty} \alpha_n |n\rangle_A |n\rangle_B, \end{aligned} \quad (3)$$

where

$$\hat{V}_{kl}(\theta) = \exp \left[\theta (\hat{a}_k^{\dagger} \hat{a}_l - \hat{a}_k \hat{a}_l^{\dagger}) \right] \quad (4)$$

is the beam splitter operator, and the parameter θ is related to the transmittance T as

$$\tan \theta = \sqrt{\frac{1-T}{T}}, \quad (5)$$

and $\theta = \pi/4$ corresponds to the balanced beam splitter. The operator $\hat{S}_{kl}^{(2)}(r)$ is the two-mode squeezing operator,

$$\hat{S}_{kl}^{(2)}(r) = \exp \left[-r (\hat{a}_k^{\dagger} \hat{a}_l^{\dagger} - \hat{a}_k \hat{a}_l) \right]. \quad (6)$$

Introducing $\lambda \equiv \tanh r$, the Schmidt coefficients are given by

$$\alpha_n = \sqrt{1 - \lambda^2} \lambda^n. \quad (7)$$

The beam at path C (D) is then tapped off from path A (B) by a beam splitter of transmittance T . We set

$T = 0.9$ throughout this paper. The resulting four-mode state just after the second beam splitters is

$$\begin{aligned} |\psi\rangle_{ABCD} &= \hat{V}_{BD}(\theta)\hat{V}_{AC}(\theta)|r^{(2)}\rangle_{AB}|0\rangle_{CD} \\ &= \sum_n \alpha_n \sum_{i,j=0}^n \xi_{ni}\xi_{nj}|n-i\rangle_A|n-j\rangle_B|i\rangle_C|j\rangle_D, \end{aligned} \quad (8)$$

where

$$\xi_{nk} = (-1)^k \sqrt{\binom{n}{k}} (\sqrt{T})^{n-k} (\sqrt{R})^k, \quad (9)$$

and $\binom{n}{k}$ is the binomial coefficient and $R = 1 - T$ is the reflectance.

A. Photon number resolving detector case

When k (l) photons are detected in the beam at path C (D) by an ideal photon number resolving detector, the conditional state is given by

$$\begin{aligned} |\psi_{\text{NG}}^{(kl)}\rangle_{AB} &\propto {}_D\langle l|_C\langle k|\psi\rangle_{ABCD} \\ &= \sum_{n=\max\{k,l\}}^{\infty} \alpha_n \xi_{nk} \xi_{nl} |n-k\rangle_A |n-l\rangle_B, \end{aligned} \quad (10)$$

where $|\psi_{\text{NG}}\rangle_{AB}$ is still a pure state. In the case of $k = l = 1$,

$$\begin{aligned} |\psi_{\text{NG}}^{(1)}\rangle_{AB} &= \frac{1}{\sqrt{P_{\text{det}}^{(1)}}} \sum_{n=0}^{\infty} \alpha_{n+1} \xi_{(n+1),1}^2 |n\rangle_A |n\rangle_B \\ &= \sum_{n=0}^{\infty} c_n^{(1)} |n\rangle_A |n\rangle_B, \end{aligned} \quad (11)$$

where

$$\begin{aligned} P_{\text{det}}^{(1)} &= \sum_{n=0}^{\infty} |\alpha_{n+1}|^2 |\xi_{(n+1),1}^2|^2 \\ &= \frac{(1-\lambda^2)\lambda^2 T^2 (1+\lambda^2 T^2)}{(1-\lambda^2 T^2)^3} \left(\frac{R}{T}\right)^2 \end{aligned} \quad (12)$$

is the probability of detecting one photon in each arm. The state (11) is *not* Gaussian any more.

B. On/off type detector case

An ideal on/off type detector is described by a positive operator-valued measure (POVM) with elements

$$\begin{cases} \hat{\Pi}^{(\text{off})} &= |0\rangle\langle 0|, \\ \hat{\Pi}^{(\text{on})} &= |1\rangle\langle 1| + |2\rangle\langle 2| + \dots = \hat{1} - |0\rangle\langle 0|. \end{cases} \quad (13)$$

The two-mode squeezed state is transformed into a mixed non-Gaussian state

$$\begin{aligned} \hat{\rho}_{\text{NG}} &= \frac{\text{Tr}_{CD} \left[|\psi\rangle_{(ABCD)} \langle \psi| \otimes \left(\hat{\Pi}_C^{(\text{on})} \otimes \hat{\Pi}_D^{(\text{on})} \right) \right]}{\mathcal{P}_{\text{det}}} \\ &= \frac{1}{\mathcal{P}_{\text{det}}} \sum_{i,j=1}^{\infty} |\Phi_{ij}\rangle_{(AB)} \langle \Phi_{ij}|, \end{aligned} \quad (14)$$

where

$$|\Phi_{ij}\rangle_{AB} = \sum_{n=\max\{i,j\}} \alpha_n \xi_{ni} \xi_{nj} |n-i\rangle_A |n-j\rangle_B, \quad (15)$$

and \mathcal{P}_{det} is the probability of detecting at least one photon in each of the paths C and D,

$$\begin{aligned} \mathcal{P}_{\text{det}} &= \text{Tr}_{ABCD} \left[|\psi\rangle_{(ABCD)} \langle \psi| \otimes \left(\hat{\Pi}_C^{(\text{on})} \otimes \hat{\Pi}_D^{(\text{on})} \right) \right] \\ &= \frac{\lambda^2 (1-T)^2 (1+\lambda^2 T)}{(1-\lambda^2 T)(1-\lambda^2 T^2)}. \end{aligned} \quad (16)$$

The mean photon number of the state $\hat{\rho}_{\text{NG}}$ is expressed as

$$\begin{aligned} \bar{N}_{\text{NG}} &= \text{Tr}_{AB} \left[\hat{\rho}_{\text{NG}} \otimes \left(\hat{N}_A + \hat{N}_B \right) \right] \\ &= \frac{2(1-\lambda^2)}{\mathcal{P}_{\text{det}}} \left[\frac{\lambda^2 T}{(1-\lambda^2)^2} - \frac{\lambda^2 T}{(1-\lambda^2 T^2)^2} \right. \\ &\quad \left. - \frac{\lambda^2 T^2}{(1-\lambda^2 T)^2} + \frac{\lambda^2 T^2}{(1-\lambda^2 T^2)^2} \right], \end{aligned} \quad (17)$$

which is shown in Fig. 2 as a function of λ , and used later. Here, the mean photon number of the two-mode squeezed vacuum state $\bar{N}_{\text{SQ}} = 2\lambda^2/(1-\lambda^2)$ is also shown. Note that the increase of the mean photon number for the photon-subtracted squeezed state is due to the fact that the generation process is based on the event selection of the components of higher numbers of photons by excluding the original vacuum component of the input two-mode squeezed state.

III. COMPUTABLE ENTANGLEMENT MEASURES

In this section, we briefly review the negativity and the logarithmic negativity as computable entanglement measures that possess the properties of an entanglement monotone [30]: (i) The entanglement measure E is a non-negative functional, $E(\hat{\rho}) \geq 0$, (ii) if $\hat{\rho}$ is separable, $E(\hat{\rho}) = 0$, and (iii) $E(\hat{\rho})$ does not increase *on average* under the LOCC.

The negativity of a bipartite mixed state $\hat{\rho}$, denoted by $\mathcal{N}(\hat{\rho})$, is defined as the absolute value of the sum of the negative eigenvalues of $\hat{\rho}^{PT}$, the partial transpose of $\hat{\rho}$ with respect to either subsystem. We may write this as

$$\mathcal{N}(\hat{\rho}) = \frac{1}{2} \text{Tr} \left(\sqrt{(\hat{\rho}^{PT})^2} - \hat{\rho}^{PT} \right) = \frac{\|\hat{\rho}^{PT}\| - 1}{2}, \quad (18)$$

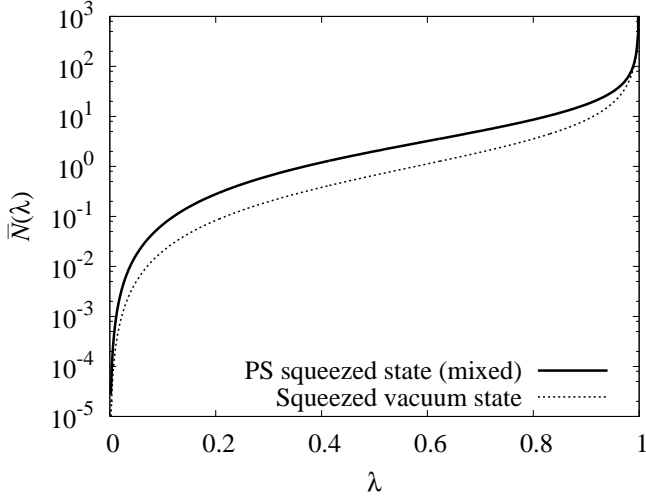


FIG. 2: Mean photon number of the photon-subtracted mixed state (thick solid line) and original two-mode squeezed vacuum state (dotted line).

where $\|\cdot\|$ denotes the trace-norm. The negativity \mathcal{N} is clearly a non-negative functional. For a separable state, $\hat{\rho} = \sum_i p_i \hat{\rho}_{Ai} \otimes \hat{\rho}_{Bi}$, the partial transpose with respect to either subsystem, say B, is given by $\hat{\rho} = \sum_i p_i \hat{\rho}_{Ai} \otimes \hat{\rho}_{Bi}^T$. This is also a state, and it therefore has zero negativity. Furthermore, under LOCC, \mathcal{N} does not increase on average [30, 35]. It is also convex, i.e.

$$\sum_i p_i \mathcal{N}(\hat{\rho}_i) \leq \mathcal{N}(\hat{\rho}), \quad (19)$$

where $\hat{\rho} = \sum_i p_i \hat{\rho}_i$. The logarithmic negativity is defined as

$$E_{\mathcal{N}}(\hat{\rho}) = \log_2(1 + 2\mathcal{N}(\hat{\rho})) = \log_2(\|\hat{\rho}^{PT}\|). \quad (20)$$

In addition to the properties (i), (ii), and (iii), this quantity is additive because $\|\hat{\rho}^{PT} \otimes \hat{\sigma}^{PT}\| = \|\hat{\rho}^{PT}\| \cdot \|\hat{\sigma}^{PT}\|$, which is also a desired property of a good entanglement measure.

For a pure entangled state

$$|\chi\rangle_{AB} = \sum_n c_n |n\rangle_A |n\rangle_B, \quad (21)$$

the negativity and the logarithmic negativity can be calculated analytically, where, without loss of generality, we take the Schmidt coefficients c_n to be non-negative. We use the fact that

$$\left\| \{ |\chi\rangle_{(AB)} \langle \chi| \}^{PT} \right\| = \left(\sum_n c_n \right)^2, \quad (22)$$

and we can obtain [30]:

$$\mathcal{N}(\chi) = \frac{(\sum_n c_n)^2 - 1}{2}, \quad (23)$$

$$E_{\mathcal{N}}(\chi) = 2 \log_2 \left(\sum_n c_n \right) \quad (24)$$

For mixed states, it is typically not possible to obtain analytical expressions for the negativity and the logarithmic negativity. However, they can often be numerically computable using linear algebra packages.

IV. NUMERICAL EVALUATION OF NEGATIVITIES

In this section, we explain the procedure for numerical evaluation of the negativities of the photon-subtracted squeezed state with the on/off detectors. First, we expand the output non-Gaussian state (14) in the Fock basis,

$$\hat{\rho}_{\text{NG}} = \sum_{m_1, m_2, n_1, n_2} \rho_{m_1 m_2 n_1 n_2} |m_1\rangle_A \langle m_2| \otimes |n_1\rangle_B \langle n_2|, \quad (25)$$

where

$$\begin{aligned} & \rho_{m_1 m_2 n_1 n_2} \\ &= {}_B \langle n_1 | {}_A \langle m_1 | \hat{\rho}_{\text{NG}} | m_2 \rangle_A | n_2 \rangle_B \\ &= \frac{1}{\mathcal{P}_{\text{det}}} \sum_{i,j=1}^{\infty} \alpha_{m_1+i} \alpha_{m_2+i} \xi_{(m_1+i),i} \xi_{(m_1+i),j} \\ & \quad \times \xi_{(m_2+i),i} \xi_{(m_2+i),j} \delta_{(m_1-n_1),(j-i)} \delta_{(m_2-n_2),(j-i)}, \end{aligned} \quad (26)$$

which means that the density matrix elements are zero unless $m_1 - n_1 = m_2 - n_2$.

The partial transpose of this state, with respect to mode B, is

$$\hat{\rho}_{\text{NG}}^{PT} = \sum_{m_1, m_2, n_1, n_2} \rho_{m_1 m_2 n_2 n_1} |m_1\rangle_A \langle m_2| \otimes |n_1\rangle_B \langle n_2|, \quad (27)$$

where the elements are zero unless $m_1 + n_1 = m_2 + n_2 = K$. The parameter K is the total photon number of both beams at paths A and B, and the partially-transposed density operator is block diagonal in Fock state basis, where the blocks correspond to $K = 0, 1, 2, \dots$:

$$\hat{\rho}_{\text{NG}}^{PT} = \bigoplus_{K=0}^{\infty} \hat{\rho}_{\text{NG}}^{PT}(K). \quad (28)$$

Here, $\hat{\rho}_{\text{NG}}^{PT}(K)$ is the K -th submatrix which is a $(K+1) \times (K+1)$ real matrix (Fig. 3).

The eigenvalues are obtained by numerically diagonalizing the partially transposed density matrix,

$$\hat{\rho} = \hat{U}^T \hat{\rho}_{\text{NG}}^{PT} \hat{U}, \quad (29)$$

which can separately be done for every submatrix one by one,

$$\begin{aligned} \hat{\rho}_K &= \hat{U}_K^T \hat{\rho}_{\text{NG}}^{PT}(K) \hat{U}_K \\ &= \sum_{l=0}^K \omega_l^K |K-l\rangle_A \langle K-l| \otimes |l\rangle_B \langle l|, \end{aligned} \quad (30)$$

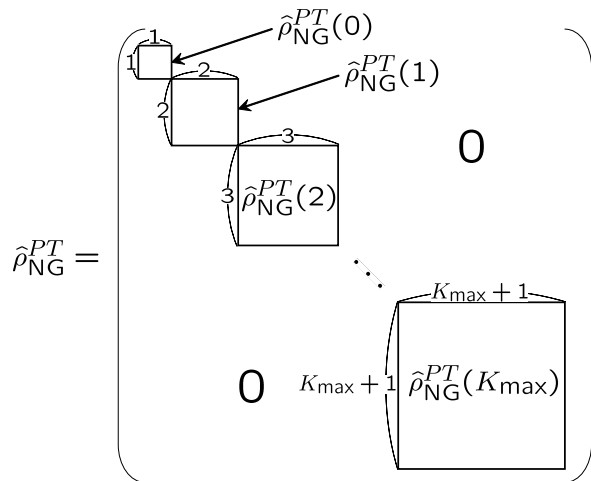


FIG. 3: Partially-transposed density matrix of the photon-subtracted mixed state with the cut-off K_{max} , which is block diagonal in Fock state basis.

where ω_l^K is the l -th eigenvalue of K -th submatrix, and

$$\hat{U} = \bigoplus_{K=0}^{\infty} \hat{U}_K. \quad (31)$$

In the numerical calculation, we introduce a cut-off K_{max} , which must be large enough compared with the mean photon number. Then, we sum up all the negative eigenvalues, which gives the negativity,

$$\mathcal{N}(\hat{\rho}_{\text{NG}}) = \frac{1}{\Delta_{K_{\text{max}}}} \sum_{K=0}^{K_{\text{max}}} \sum_{\omega_l^K < 0} |\omega_l^K|, \quad (32)$$

where

$$\Delta_{K_{\text{max}}}(\lambda) \equiv \sum_{K=0}^{K_{\text{max}}} \text{Tr} \hat{\rho}_{\text{NG}}^{\text{PT}}(K) \quad (33)$$

is the trace of the truncated density matrix. With this result, we can obtain the logarithmic negativity straightforwardly using Eq. (20).

In our computations, we chose a cut-off of $K_{\text{max}} = 50$. The trace (33) could be used as a measure of the validity of our chosen cut-off. For $\lambda = 0.78$ and 0.88 , which corresponds to $\bar{N}_{\text{NG}} \simeq 7.71$ and 14.7 , $\Delta_{K_{\text{max}}=50} \simeq 1.000$ and 0.995 , respectively. For the latter case, indeed, it still misses 0.5% of the support, but this precision suffices for our analysis. In this connection, with $K_{\text{max}} = 50$, it takes 3.5 days to calculate the negativity for a certain λ , by means of a Mathematica program on Pentium 4 3.2E GHz PC (including the generation of matrix components). It is necessary to reach a satisfactory compromise between the precision of the numerical calculation and the calculation cost. The numerical calculation becomes progressively time-consuming with increasing K_{max} .

Figures 4 and 5 show the numerical values of the negativity and the logarithmic negativity, respectively.

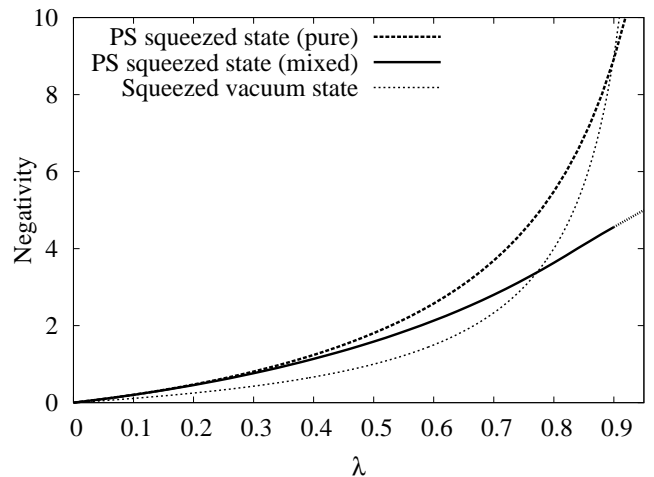


FIG. 4: Negativity of the photon-subtracted squeezed states, in pure state case (thick dashed line) and mixed state case (thick solid line). The dotted line corresponds to the input squeezed vacuum.

The thick dashed line represents the photon-subtracted squeezed state of the pure state case (11), while the thick solid line corresponds to the mixed one (14). The dotted line is for the input two-mode squeezed vacuum (3). Using the expression in Eq. (7) for the Schmidt coefficients of the squeezed vacuum state, we find, from Eqs. (23) and (24), that the negativity and logarithmic negativity of this state are given by

$$\mathcal{N}(\lambda) = \frac{\lambda}{1-\lambda}, \quad (34)$$

$$E_{\mathcal{N}}(\lambda) = \log_2(1+\lambda) - \log_2(1-\lambda). \quad (35)$$

As can be seen in the figures, the photon subtracted non-Gaussian states have a larger amount of entanglement than the input two-mode squeezed vacuum state in a practical squeezing range, $\lambda \lesssim \lambda_{\text{LN}}^{\text{P}} = 0.897$ for the pure state case, and $\lambda \lesssim \lambda_{\text{LN}}^{\text{M}} = 0.772$ for the mixed one, which correspond to 8.9 dB and 7.1 dB ideal squeezing. Exceeding these λ_{LN} 's, however, the merit of non-Gaussian operation disappears. For $\lambda \lesssim 0.2$, that is, $\bar{N}_{\text{NG}} \lesssim 0.28$, the difference between the cases of the photon number resolving detector and the on/off type detector is almost negligible compared with the difference between them in the case of ideal two-mode squeezed state. This means that the photon subtraction by a beam splitter of transmittance $T = 0.9$ and the on/off detectors emulate the single photon subtraction well.

V. OPERATIONAL ENTANGLEMENT MEASURES

In this section, we review the previous results on the operational entanglement measures, and compare them with the above results of logarithmic negativity.

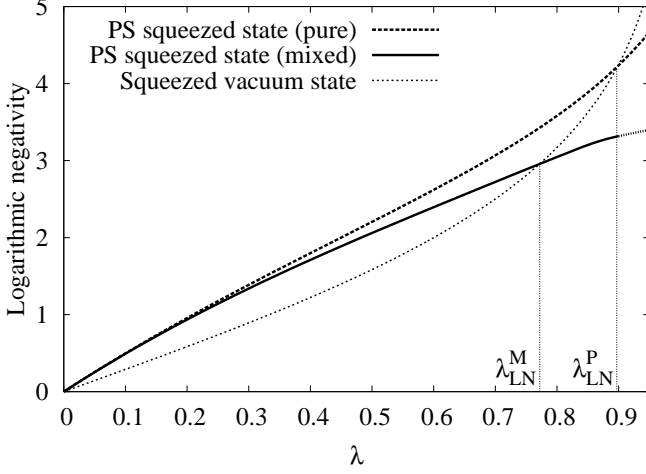


FIG. 5: The same plot as Fig. 4 of the logarithmic negativity. The values of each intersection are $\lambda_{\text{LN}}^{\text{P}} \simeq 0.897$ and $\lambda_{\text{LN}}^{\text{M}} \simeq 0.772$.

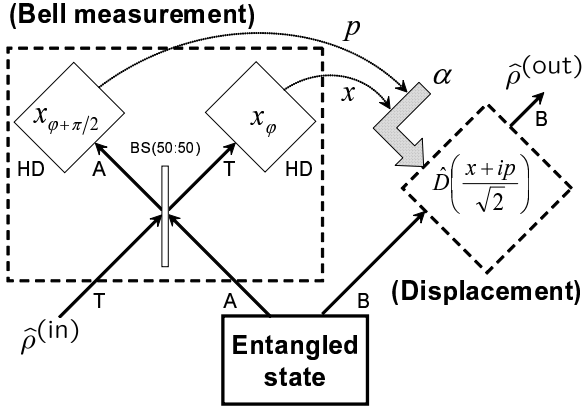


FIG. 6: CV teleportation scheme. BS and HD mean the beam splitter and homodyne detection, respectively.

A. CV teleportation fidelity

The first operational measure is the CV teleportation fidelity [20]. In quantum teleportation, an unknown quantum state can be transferred using entanglement and a classical channel. The schematic is shown in Fig. 6. First, the sender Alice and the receiver Bob share the entangled state $\hat{\rho}_{\text{AB}}^{(\text{E})}$. Alice then performs the Bell measurement, that is, a projective measurement in the maximally entangled basis

$$|\Pi(x, p)\rangle_{kl} = \frac{1}{\sqrt{2\pi}} \int_{-\infty}^{\infty} dy e^{ipy} |x+y\rangle_k |y\rangle_l \quad (36)$$

upon the unknown state $\hat{\rho}_{\text{T}}^{(\text{in})}$ and her fragment of entangled state (A). She obtains a couple of measurement results (x, p) , and Bob's part of the initial state (B) is

correspondingly transformed into

$$\hat{\sigma}_{\text{B}}(x, p) = \frac{{}_{\text{TA}}\langle \Pi(x, p) | [\hat{\rho}_{\text{T}}^{(\text{in})} \otimes \hat{\rho}_{\text{AB}}^{(\text{E})}] | \Pi(x, p) \rangle_{\text{TA}}}{P^{(\text{tlp})}(x, p)}, \quad (37)$$

where

$$P^{(\text{tlp})}(x, p) = \text{Tr}_{\text{B}} \left[{}_{\text{TA}}\langle \Pi(x, p) | [\hat{\rho}_{\text{T}}^{(\text{in})} \otimes \hat{\rho}_{\text{AB}}^{(\text{E})}] | \Pi(x, p) \rangle_{\text{TA}} \right] \quad (38)$$

is the Bell measurement probability distribution. Finally, Bob corrects his state with the unitary transformation, that is, the displacement operation $\hat{D}(\alpha) = \exp[\alpha \hat{a}^\dagger - \alpha^* \hat{a}]$ according to Alice's measurement result,

$$\hat{\rho}_{\text{B}}^{(\text{out})}(x, p) = \hat{D} \left(\frac{x + ip}{\sqrt{2}} \right) \hat{\sigma}_{\text{B}}(x, p) \hat{D}^\dagger \left(\frac{x + ip}{\sqrt{2}} \right). \quad (39)$$

The average fidelity between the input and output is

$$\bar{F} = \int_{-\infty}^{\infty} dx \int_{-\infty}^{\infty} dp P^{(\text{tlp})}(x, p) \text{Tr} \left[\hat{\rho}_{\text{T}}^{(\text{in})} \hat{\rho}^{(\text{out})}(x, p) \right], \quad (40)$$

which depends upon the input state $\hat{\rho}_{\text{T}}^{(\text{in})}$. Let us consider that the input state is the coherent state,

$$\hat{\rho}_{\text{T}}^{(\text{in})} = |\alpha_0\rangle_{\text{T}} \langle \alpha_0|, \quad (41)$$

which is one of the unaffected state. With the two-mode squeezed vacuum state (3), the average fidelity is

$$\bar{F}_{\text{SQ}}(\lambda) = \frac{1 + \lambda}{2}, \quad (42)$$

and, with the non-Gaussian pure state (11) and mixed one (14),

$$\bar{F}_{\text{NG}}^{(1)}(\lambda) = \frac{(1 - \lambda^2) \lambda^2 T^2 \left(1 - \lambda T + \frac{\lambda^2 T^2}{2} \right)}{2 P_{\text{det}}^{(1)} (1 - \lambda T)^3} \left(\frac{R}{T} \right)^2, \quad (43)$$

$$\bar{F}_{\text{NG}}(\lambda) = \mathcal{F}_{11}(\lambda) - \mathcal{F}_{10}(\lambda) - \mathcal{F}_{01}(\lambda) + \mathcal{F}_{00}(\lambda), \quad (44)$$

respectively, where

$$\mathcal{F}_{ij}(\lambda) = \frac{1}{2 P_{\text{det}}^{(1)}} \frac{1 - \lambda^2}{1 - \lambda T - \lambda^2 \gamma_i \gamma_j - \frac{\lambda^2 T}{2} (\gamma_i + \gamma_j)} \quad (45)$$

and $\gamma_1 = R$, $\gamma_0 = 0$. See appendix A and B for more detail derivations.

Figure 7 shows the average fidelities. We can see that the photon-subtracted squeezed states, both the pure and mixed cases, are superior to the original squeezed vacuum state for $\lambda \lesssim \lambda_{\text{T}}^{\text{P}} = 0.815$ and $\lambda \lesssim \lambda_{\text{T}}^{\text{M}} = 0.708$, respectively. In the range of $\lambda_{\text{T}}^{\text{P}} < \lambda$, on the other hand, the squeezed vacuum state shows the best performance, which is quantitatively consistent with the logarithmic negativity result. As seen by computing the result of Fig. 5 and 7, whenever the fidelity is improved by the photon subtraction, so is the logarithmic negativity. We

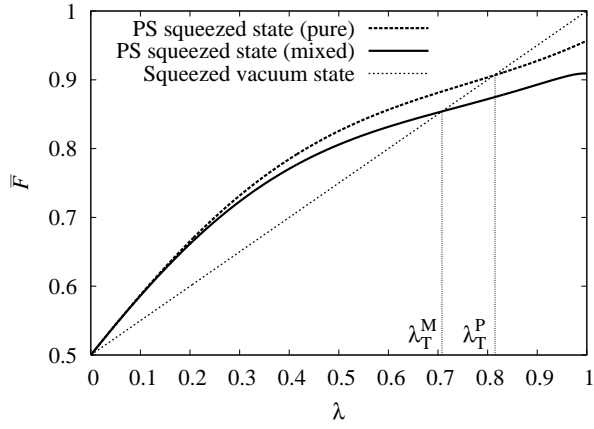


FIG. 7: Average fidelity of CV teleportation of coherent state, with the photon-subtracted pure state (thick dashed line), mixed one (thick solid line), and original squeezed vacuum state (dotted line). The values of each intersection are $\lambda_T^P \simeq 0.815$ and $\lambda_{LN}^M \simeq 0.708$.

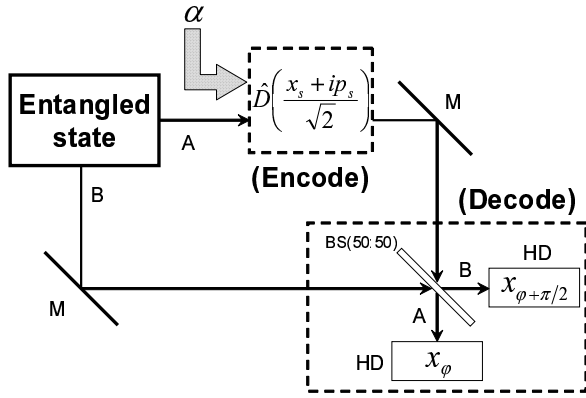


FIG. 8: CV dense coding scheme, with power of signal modulation α . BS, M, and HD mean beam splitter, mirror, and homodyne detection, respectively.

cannot, however, exclude the possibility that this is not true for other input states for the teleportation. It is still impossible to scan the fidelity for any input state. A series of CV teleportation operations may be more effective for *Gaussian* entangled state, which is another factor λ_T is different from λ_{LN} .

B. Mutual information in CV dense coding scheme

The second operational measure is the CV dense coding scheme [24]. The schematic is illustrated in Fig. 8. In this scheme, Alice and Bob share the entangled state $\hat{\rho}_{AB}^{(E)}$ initially. Then, Alice encodes *classical* message by a modulation on the beam path A,

$$\hat{U}_A(x_s, p_s) = e^{-(i/2)x_s p_s} \hat{D}\left(\frac{x_s + ip_s}{\sqrt{2}}\right) = e^{-ip_s \hat{x}_A} e^{ix_s \hat{p}_A}. \quad (46)$$

For the sake of simplicity, we consider the quaternary phase-shift keying (QPSK), with equal likelihood: $a_{00} = (x_s = \sqrt{2}\beta, p_s = \sqrt{2}\beta)$, $a_{01} = (\sqrt{2}\beta, -\sqrt{2}\beta)$, $a_{10} = (-\sqrt{2}\beta, \sqrt{2}\beta)$, $a_{11} = (-\sqrt{2}\beta, -\sqrt{2}\beta)$ for some real β , and $P(a_{kl}) = 1/4$. Bob decodes the signals by the Bell measurement (36), and the decision rule is as follows: $\{b_{00} = (x \geq 0, p \geq 0), b_{01} = (x \geq 0, p < 0), b_{10} = (x < 0, p \geq 0), b_{11} = (x < 0, p < 0)\}$. The channel matrix of CV dense coding $P^{(\text{ch})}(b_{mn}|a_{kl})$, which is the conditional probability, is calculated with the homodyne probability distribution,

$$\begin{aligned} P^{(\text{HD})}(x, p|x_s, p_s) \\ = {}_{AB} \langle \Pi(x, p) | \hat{U}_A(x_s, p_s) \hat{\rho}_{AB}^{(E)} \hat{U}_A^\dagger(x_s, p_s) | \Pi(x, p) \rangle_{AB}. \end{aligned} \quad (47)$$

For example, $P^{(\text{ch})}(b_{00}|a_{00})$ component of channel matrix is

$$P^{(\text{ch})}(b_{00}|a_{00}) = \int_0^\infty dx \int_0^\infty dp P^{(\text{HD})}(x, p|\sqrt{2}\beta, \sqrt{2}\beta), \quad (48)$$

and other components are calculated similarly. With this 4×4 channel matrix, the mutual information is calculated as

$$\begin{aligned} I(A;B) &= \sum_{k,l,m,n} P(a_{kl}) P^{(\text{ch})}(b_{mn}|a_{kl}) \\ &\times \log_2 \left[\frac{P^{(\text{ch})}(b_{mn}|a_{kl})}{\sum_{k',l'} P(a_{k'l'}) P^{(\text{ch})}(b_{mn}|a_{k'l'})} \right] [\text{bit}]. \end{aligned} \quad (49)$$

With the two-mode squeezed vacuum state (3),

$$\begin{aligned} I_{\text{SQ}}(A;B) \\ = \left[1 + \text{erf}\left(\sqrt{\frac{1+\lambda}{1-\lambda}}\beta\right) \right] \log_2 \left[1 + \text{erf}\left(\sqrt{\frac{1+\lambda}{1-\lambda}}\beta\right) \right] \\ + \left[1 - \text{erf}\left(\sqrt{\frac{1+\lambda}{1-\lambda}}\beta\right) \right] \log_2 \left[1 - \text{erf}\left(\sqrt{\frac{1+\lambda}{1-\lambda}}\beta\right) \right], \end{aligned} \quad (50)$$

where

$$\text{erf}(x) = \frac{2}{\sqrt{\pi}} \int_0^x dt e^{-t^2} \quad (51)$$

is the error function. With the non-Gaussian pure state (11),

$$\begin{aligned} I_{\text{NG}}^{(1)}(A;B) &= \frac{1}{4} (I_1 \log_2 I_1 + I_2 \log_2 I_2 \\ &\quad + I_3 \log_2 I_3 + I_4 \log_2 I_4), \end{aligned} \quad (52)$$

and

$$I_1 = \mathcal{D}_\mu \frac{1}{\mu} \left[1 + \operatorname{erf} \left(\sqrt{\frac{1+\lambda T}{1-\lambda T}} \mu \beta \right) \right]^2 \Big|_{\mu=1}, \quad (53)$$

$$I_2 = I_3 = \mathcal{D}_\mu \frac{1}{\mu} \left[1 - \operatorname{erf} \left(\sqrt{\frac{1+\lambda T}{1-\lambda T}} \mu \beta \right) \right]^2 \Big|_{\mu=1} \quad (54)$$

$$I_4 = \mathcal{D}_\mu \frac{1}{\mu} \left[1 - \operatorname{erf} \left(\sqrt{\frac{1+\lambda T}{1-\lambda T}} \mu \beta \right) \right]^2 \Big|_{\mu=1} \quad (55)$$

where

$$\mathcal{D}_\mu = \frac{(1-\lambda^2)\lambda^2 T^2}{P_{\det}^{(1)}(1-\lambda T)^2(1-\lambda^2 T^2)} \left(\frac{R}{T} \right)^2 \times \left[\left(\frac{\lambda T}{1+\lambda T} \right)^2 \frac{\partial^2}{\partial \mu^2} + \frac{2\lambda T}{1+\lambda T} \frac{\partial}{\partial \mu} + 1 \right] \quad (56)$$

is the differential operator with respect to the auxiliary parameter μ . With the non-Gaussian mixed state (14),

$$\mathcal{I}_{\text{NG}}(A;B) = \frac{1}{4} (\mathcal{I}_1 \log_2 \mathcal{I}_1 + \mathcal{I}_2 \log_2 \mathcal{I}_2 + \mathcal{I}_3 \log_2 \mathcal{I}_3 + \mathcal{I}_4 \log_2 \mathcal{I}_4), \quad (57)$$

where

$$\mathcal{I}_1 = \sum_{i,j=0}^1 (-1)^{i+j} \mathcal{C}_{ij} [1 + \operatorname{erf}(\Omega_{ij}\beta)]^2, \quad (58)$$

$$\mathcal{I}_2 = \mathcal{I}_3 = \sum_{i,j=0}^1 (-1)^{i+j} \mathcal{C}_{ij} [1 - \operatorname{erf}(\Omega_{ij}\beta)]^2, \quad (59)$$

$$\mathcal{I}_4 = \sum_{i,j=0}^1 (-1)^{i+j} \mathcal{C}_{ij} [1 - \operatorname{erf}(\Omega_{ij}\beta)]^2, \quad (60)$$

and

$$\mathcal{C}_{ij} = \frac{1-\lambda^2}{1-\lambda^2(T+\gamma_i)(T+\gamma_j)}, \quad (61)$$

$$\Omega_{ij} = \sqrt{\frac{1-\lambda^2(T+\gamma_i)(T+\gamma_j)}{(1-\lambda T)^2 - \lambda^2 \gamma_i \gamma_j}}, \quad (62)$$

where $\gamma_1 = R$ and $\gamma_0 = 0$ as before. See appendix A and B for more detail derivations.

In Figs. 9 and 10, the mutual information with the photon-subtracted squeezed states and the squeezed vacuum state are shown, at $\beta = 1.5$ and 0.7 , respectively.

From these results, we can see that the range of λ for which the non-Gaussian operation brings the gain to the mutual information becomes wide as β becomes small. When β gets smaller, the overlap between the probability distributions of different signals increases, and the distinction of encoded signals becomes more difficult. Just in this situation, we can see the *bona fide* effect of entanglement in CV dense coding scheme. As $\beta \rightarrow 0$, the

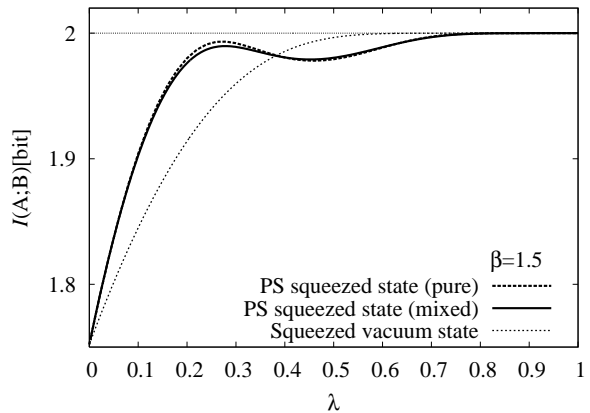


FIG. 9: Mutual information in dense coding scheme with the photon-subtracted pure state (dashed line), mixed one (solid line), and squeezed vacuum state (dotted line) at $\beta = 1.5$.

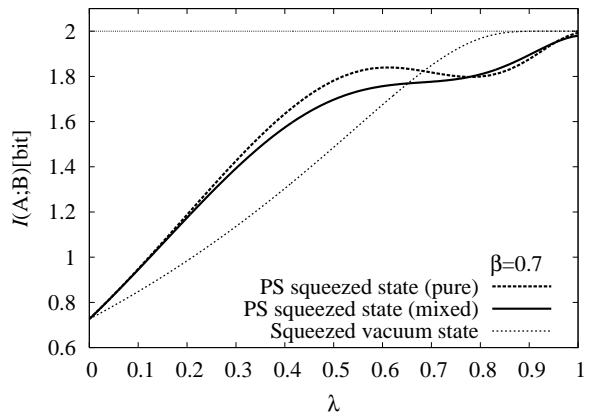


FIG. 10: The same plot as Fig. 9 at $\beta = 0.7$.

intersections of the curves for the non-Gaussian states and the squeezed vacuum state approach $\lambda_D^P \simeq 0.894$ and $\lambda_D^M \simeq 0.762$, respectively (Fig. 11). These intersections are quite close to those of the logarithmic negativity. This is consistent with the logarithmic negativity result in the meaning that the mutual information indicates the range for which non-Gaussian operation enhances the entanglement.

VI. DISCUSSION AND CONCLUSION

In this paper, we have studied how to quantify the entanglement of the non-Gaussian mixed state which is generated by the photon subtraction from the two-mode squeezed vacuum state. In order to enhance the entanglement of a given Gaussian state at distant sites by the LOCC, no Gaussian operations suffice. When the photon subtraction is made by the on/off detector, the resulting state is generally a mixed state. Evaluating the entanglement of such a state is far from trivial.

We have applied the negativity and the logarithmic

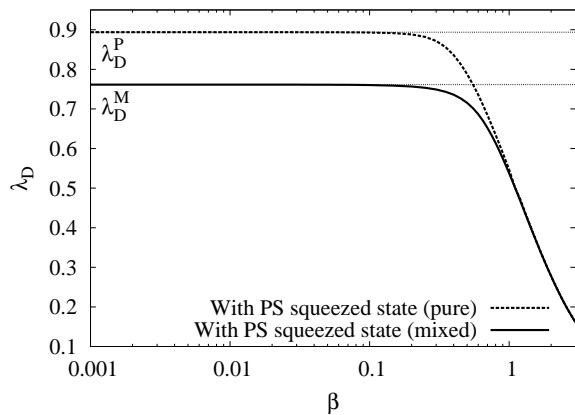


FIG. 11: Intersections of the input squeezed state curve and photon-subtracted squeezed state curves. It converges to $\lambda_D^P \simeq 0.894$ for the pure state case, and $\lambda_D^M \simeq 0.762$ for mixed one, as $\beta \rightarrow 0$.

negativity, which is known as an entanglement monotone, to this problem. We have compared the gain measured by these measures with the one by the protocol-specific operational measures, i.e., the teleportation fidelity and the mutual information of the dense coding. Up to a certain point of λ , the photon-subtracted squeezed states, both the pure and mixed states, are superior to the input squeezed state with respect to all the measures. Exceeding this point λ , the non-Gaussian operation brings no gain, and the entangled squeezed state shows the better performance. When λ approaches unity, the effect of the non-Gaussian operation for entanglement enhancement gets lost. This is because the initial squeezed state approaches the maximally entangled EPR state, as $\lambda \rightarrow 1$, whose entanglement cannot be enhanced by any physical process.

While the operational measures have clear physical meanings, they directly depend on the input state characteristics, and the evaluation based on them vary for the protocols. The (logarithmic) negativity is, on the other hand, independent of any such external parameters. This quantity reflects the entanglement as an intrinsic property of the state itself. We have found that whenever the enhancement is seen in terms of the operational measures, the negativity and the logarithmic negativity are also enhanced. For the dense coding scheme, in particular, the upper limit of λ below which the non-Gaussian operational gain can be seen, λ_D^P (pure state case) and λ_D^M (mixed state case) approach the ones measured by the logarithmic negativity λ_{LN}^P and λ_{LN}^M , respectively, as the modulation signal power β gets smaller. It would be interesting to investigate whether the intersections λ_D in the dense coding as well as λ_T for the teleportation are identical to λ_{LN} or not after the operational measures are further optimized with respect to all the possibilities for external parameters of input states. In other words, the logarithmic negativity, not containing any additional parameter, might give the universal upper limit for the

region of λ , where the gain by the non-Gaussian operation can be seen.

The operational meaning of the logarithmic negativity has not completely been clear yet. The relationship between the logarithmic negativity and other entanglement measures, such as the entanglement of formation, has not yet been fully elucidated. Restricted to the case of symmetric Gaussian entangled states only, they always indicate the same ordering [36]. Generally, however, they could give the different ordering for a few cases [37]. Our findings will provide some insight into further studies of the evaluation of the performance of the non-Gaussian operations.

For practical application of our results to the laboratory experiment, various imperfections should be considered, such as the limited quantum efficiency and nonzero dark count rate of the photodetector, and linear loss in the optical paths. Then the logarithmic negativity evaluation in consideration of these imperfections is the important issue. However, those effects cause the complex mixing between two modes A and B. Therefore, it is not obvious whether the partially-transposed density matrix $\hat{\rho}_{NG}^{PT}$ can be split into series of submatrices, as in the case of the ideal setup. This would make the analysis much harder even by numerical simulation. Such analysis for more practical situations is a future problem.

Acknowledgments

The authors would like to M. Ban for valuable discussions.

APPENDIX A: DERIVATION OF (43) AND (52)

Let us describe the non-Gaussian pure state with coherent basis, which is suitable for inner products with both Fock state basis and continuous variable basis.

$$\langle n|\alpha\rangle = e^{-\frac{|\alpha|^2}{2}} \frac{\alpha^n}{\sqrt{n!}}, \quad (\text{A1})$$

$$\langle x|\alpha\rangle = \frac{1}{\sqrt[4]{\pi}} \exp\left[-\frac{x^2}{2} + \sqrt{2}x\alpha - \frac{\alpha^2}{2} - \frac{|\alpha|^2}{2}\right]. \quad (\text{A2})$$

First, we consider the average fidelity in CV teleportation. With coherent state basis, the pure non-Gaussian

state (11) is expressed with an auxiliary parameter μ ,

$$\begin{aligned}
& |\psi_{\text{NG}}^{(1)}\rangle_{\text{AB}} \\
&= \frac{\sqrt{1-\lambda^2}}{\pi^2 \sqrt{P_{\text{det}}^{(1)}}} \int d^2\alpha \int d^2\beta R\alpha\beta \\
&\quad \times \exp\left[-\frac{1+R}{2}(|\alpha|^2 + |\beta|^2) + \lambda\alpha^*\beta^*\right] \\
&\quad \quad \quad |\sqrt{T}\alpha\rangle_{\text{A}}|\sqrt{T}\beta\rangle_{\text{B}} \\
&= \frac{R\sqrt{1-\lambda^2}}{\pi^2 \sqrt{P_{\text{det}}^{(1)}}} \frac{\partial}{\partial\mu} \int d^2\alpha \int d^2\beta \\
&\quad \times \exp\left[-\frac{1+R}{2}(|\alpha|^2 + |\beta|^2) + \lambda\alpha^*\beta^* + \mu\alpha\beta\right] \\
&\quad \quad \quad |\sqrt{T}\alpha\rangle_{\text{A}}|\sqrt{T}\beta\rangle_{\text{B}} \Bigg|_{\mu=0}, \quad (\text{A3})
\end{aligned}$$

where $P_{\text{det}}^{(1)}$ is given by (12), and the auxiliary parameter μ should be set to zero after all integration and differential operations. The inner product between the input state $|\alpha_0\rangle$ and unnormalized output state after teleportation operation is

$$\begin{aligned}
& {}_{\text{B}}\langle\alpha_0|\sqrt{P_{\text{NG}}^{(\text{tlp})}}|\psi_{\text{out}}\rangle_{\text{B}} \\
&= {}_{\text{B}}\langle\alpha_0|_{\text{TA}}\langle\Pi(x,p)|\hat{D}(\xi)|\alpha_0\rangle_{\text{T}}|\psi_{\text{NG}}^{(1)}\rangle_{\text{AB}} \\
&= \frac{R\sqrt{1-\lambda^2}}{\sqrt{2\pi P_{\text{det}}}} \frac{\partial}{\partial\mu} \frac{1}{1-\lambda\mu} \\
&\quad \times \exp\left[-\left(1-\frac{\lambda T}{1-\lambda\mu}\right)|Q|^2 + \frac{i}{2}xp\right] \Bigg|_{\mu=0}, \quad (\text{A4})
\end{aligned}$$

where

$$Q = \frac{x+ip}{\sqrt{2}} - \alpha_0 \equiv \xi - \alpha_0. \quad (\text{A5})$$

Therefore the (x,p) component of the fidelity is

$$\begin{aligned}
& P_{\text{NG}}^{(\text{tlp})} F_{\text{NG}}^{(1)}(x,p) \\
&= \frac{R^2(1-\lambda^2)}{2\pi P_{\text{det}}^{(1)}} \frac{\partial^2}{\partial\mu_1\partial\mu_2} \frac{1}{(1-\lambda\mu_1)(1-\lambda\mu_2)} \\
&\quad \times \exp\left[-\left(2-\frac{\lambda T}{1-\lambda\mu_1}-\frac{\lambda T}{1-\lambda\mu_2}\right)|Q|^2\right] \Bigg|_{\mu_1=\mu_2=0}. \quad (\text{A6})
\end{aligned}$$

By integrating Eq. (A6) with respect to x and p , we obtain the average fidelity,

$$\begin{aligned}
& \bar{F}_{\text{NG}}^{(1)}(\lambda) \\
&= \int_{-\infty}^{\infty} dx \int_{-\infty}^{\infty} dp P_{\text{NG}}^{\text{tlp}} F_{\text{NG}}^{(\text{tlp})}(x,p) \\
&= \frac{(1-\lambda^2)\lambda^2 T^2 \left(1-\lambda T + \frac{\lambda^2 T^2}{2}\right)}{2P_{\text{det}}^{(1)}(1-\lambda T)^3} \left(\frac{R}{T}\right)^2, \quad (\text{A7})
\end{aligned}$$

which is independent of the parameter α_0 .

Then, we consider the mutual information of CV dense coding channel.

$$\begin{aligned}
& {}_{\text{AB}}\langle\Pi(x,p)|\hat{U}_{\text{A}}(x_s,p_s)|\psi_{\text{NG}}^{(1)}\rangle_{\text{AB}} e^{-ip_s(x-x_s)} \\
&= \sqrt{\frac{1-\lambda^2}{2\pi^5 P_{\text{det}}^{(1)}}} \int d^2\alpha \int d^2\beta \\
&\quad \exp\left[-(|\alpha|^2 + |\beta|^2) + \lambda\alpha^*\beta^* + T\alpha\beta\right. \\
&\quad \quad \quad \left. + \sqrt{T}\xi'^*\alpha - \sqrt{T}\xi'\beta - \frac{x^2}{2} + \frac{\xi'^2}{2}\right] R\alpha\beta \\
&= \sqrt{\frac{1-\lambda^2}{2\pi^5 P_{\text{det}}^{(1)}}} \frac{R}{T} \frac{\partial}{\partial\mu'} \int d^2\alpha \int d^2\beta \\
&\quad \exp\left[-(|\alpha|^2 + |\beta|^2) + \lambda\alpha^*\beta^* + \mu'\alpha\beta\right. \\
&\quad \quad \quad \left. + \sqrt{T}\xi'^*\alpha - \sqrt{T}\xi'\beta - \frac{x^2}{2} + \frac{\xi'^2}{2}\right] \Bigg|_{\mu'=T} \\
&= \sqrt{\frac{1-\lambda^2}{2\pi P_{\text{det}}^{(1)}}} \frac{R}{T} \frac{\lambda T}{(1-\lambda T)^2} \left[-\frac{\lambda T}{1-\lambda T}|\xi'|^2 + 1\right] \\
&\quad \times \exp\left[-\frac{\lambda T}{1-\lambda T}|\xi'|^2 - \frac{(x-x_s)^2}{2} + \frac{\xi'^2}{2}\right], \quad (\text{A8})
\end{aligned}$$

where we use the relation

$$\hat{U}_{\text{A}}(x_s,p_s)|\Pi(x,p)\rangle_{\text{AB}} = e^{-ip_s(x-x_s)}|\Pi(x-x_s,p-p_s)\rangle_{\text{AB}}, \quad (\text{A9})$$

and

$$\xi' = \frac{(x-x_s) + i(p-p_s)}{\sqrt{2}} \equiv \xi - \xi_s. \quad (\text{A10})$$

The auxiliary parameter $\mu' (= \mu + T)$ should be set to T after all integration and differential operations. From above, we obtain the homodyne probability distribution,

$$\begin{aligned}
& P_{\text{NG}}^{(\text{HD})}(x,p|x_s,p_s) \\
&= \left| {}_{\text{AB}}\langle\Pi(x,p)|\hat{U}_{\text{A}}(x_s,p_s)|\psi_{\text{NG}}^{(1)}\rangle_{\text{AB}} \right|^2 \\
&= \frac{1-\lambda^2}{2\pi P_{\text{det}}^{(1)}} \frac{\lambda^2 T^2}{(1-\lambda T)^4} \left(\frac{R}{T}\right)^2 \left[-\frac{\lambda T}{1-\lambda T}|\xi'|^2 + 1\right]^2 \\
&\quad \times \exp\left[-\frac{1+\lambda T}{1-\lambda T}|\xi'|^2\right] \\
&= \frac{1-\lambda^2}{2\pi P_{\text{det}}^{(1)}} \frac{\lambda^2 T^2}{(1-\lambda T)^4} \left(\frac{R}{T}\right)^2 \\
&\quad \left[\left(\frac{\lambda T}{1+\lambda T}\right)^2 \frac{\partial^2}{\partial\mu''^2} + \frac{2\lambda T}{1+\lambda T} \frac{\partial}{\partial\mu''} + 1 \right] \\
&\quad \exp\left[-\mu'' \frac{1+\lambda T}{1-\lambda T}|\xi'|^2\right] \Bigg|_{\mu''=1}, \quad (\text{A11})
\end{aligned}$$

where the auxiliary parameter μ'' should be set to unity after all differential operations. With Eq. (A11), the components of channel matrix can be calculated. For example,

$$\begin{aligned} P_{\text{NG}}^{(\text{ch})}(b_{00}|a_{00}) &= \int_0^\infty dx \int_0^\infty dp P_{\text{NG}}^{(\text{HD})}(x, p|\sqrt{2}\beta, \sqrt{2}\beta) \\ &= \frac{1}{4} \mathcal{D}_{\mu''} \frac{1}{\mu''} \left[1 + \text{erf} \left(\sqrt{\frac{1+\lambda T}{1-\lambda T}} \mu'' \beta \right) \right] \Big|_{\mu''=1} \end{aligned} \quad (\text{A12})$$

where

$$\begin{aligned} \mathcal{D}_{\mu''} &= \frac{(1-\lambda^2)\lambda^2 T^2}{P_{\text{det}}^{(1)}(1-\lambda T)^2(1-\lambda^2 T^2)} \left(\frac{R}{T} \right)^2 \\ &\times \left[\left(\frac{\lambda T}{1+\lambda T} \right)^2 \frac{\partial^2}{\partial \mu''^2} + \frac{2\lambda T}{1+\lambda T} \frac{\partial}{\partial \mu''} + 1 \right] \end{aligned} \quad (\text{A13})$$

is the differential operator with respect to the auxiliary parameter μ'' . Other components can be derived similarly. With these results, we can obtain the mutual information (52).

APPENDIX B: DERIVATION OF (44) AND (57)

Similar to the Appendix A, we describe the non-Gaussian mixed state with coherent basis,

$$\begin{aligned} \hat{\rho}_{\text{NG}} &= \frac{1-\lambda^2}{\pi^4 \mathcal{P}_{\text{det}}} \int d^2\alpha_1 \int d^2\alpha_2 \int d^2\beta_1 \int d^2\beta_2 \\ &\exp \left[-\frac{1+R}{2} (|\alpha_1|^2 + |\alpha_2|^2 + |\beta_1|^2 + |\beta_2|^2) \right. \\ &\quad \left. + \lambda(\alpha_1^* \beta_1^* + \alpha_2 \beta_2) \right] \\ &\times \left(e^{R(\alpha_1 \alpha_2^* + \beta_1 \beta_2^*)} - e^{R\alpha_1 \alpha_2^*} - e^{R\beta_1 \beta_2^*} + 1 \right) \\ &|\sqrt{T}\alpha_1\rangle_{\text{A}} \langle \sqrt{T}\alpha_2| \otimes |\sqrt{T}\beta_1\rangle_{\text{B}} \langle \sqrt{T}\beta_2| \\ &= \sum_{i,j=0}^1 (-1)^{i+j} \frac{1-\lambda^2}{\pi^4 \mathcal{P}_{\text{det}}} \int d^2\alpha_1 \int d^2\alpha_2 \int d^2\beta_1 \int d^2\beta_2 \\ &\exp \left[-\frac{1+R}{2} (|\alpha_1|^2 + |\alpha_2|^2 + |\beta_1|^2 + |\beta_2|^2) \right. \\ &\quad \left. + \lambda(\alpha_1^* \beta_1^* + \alpha_2 \beta_2) + \gamma_i \alpha_1 \alpha_2^* + \gamma_j \beta_1 \beta_2^* \right] \\ &|\sqrt{T}\alpha_1\rangle_{\text{A}} \langle \sqrt{T}\alpha_2| \otimes |\sqrt{T}\beta_1\rangle_{\text{B}} \langle \sqrt{T}\beta_2|, \end{aligned} \quad (\text{B1})$$

where \mathcal{P}_{det} is give by Eq. (16), and $\gamma_1 = R$, $\gamma_0 = 0$.

With the representation (B1), the unnormalized state

after teleportation operation is

$$\begin{aligned} \mathcal{P}_{\text{NG}}^{(\text{tlp})}(x, p) \hat{\rho}_{\text{NG}}^{(\text{out})}(x, p) &= \hat{D}_{\text{B}}(\xi)_{\text{TA}} \langle \Pi(x, p) | \left[\hat{\rho}_{\text{T}}^{(\text{in})} \otimes \hat{\rho}_{\text{AB}}^{(\text{E})} \right] | \Pi(x, p) \rangle_{\text{TA}} \hat{D}_{\text{B}}^\dagger(\xi), \\ &= \sum_{i,j} (-1)^{i+j} \frac{1-\lambda^2}{2\pi^3 \mathcal{P}_{\text{det}}} \int d^2\beta_1 \int d^2\beta_2 \\ &\exp \left[-\frac{1+R}{2} (|\beta_1|^2 + |\beta_2|^2) + \gamma_j \beta_1 \beta_2^* + \lambda^2 \gamma_i \beta_1^* \beta_2 \right. \\ &\quad \left. - \lambda \sqrt{T} Q \beta_1^* - \lambda \sqrt{T} Q^* \beta_2 - |Q|^2 \right. \\ &\quad \left. + \frac{\sqrt{T}}{2} (\xi \beta_1 - \xi^* \beta_2 + \xi^* \beta_2 - \xi^* \beta_1) \right] \\ &|\sqrt{T}\beta_1 + \xi\rangle_{\text{B}} \langle \sqrt{T}\beta_2 + \xi|, \end{aligned} \quad (\text{B2})$$

where Q and ξ are similar to the definition in Eq. (A5). Therefore, the (x, p) component of the fidelity is

$$\begin{aligned} \mathcal{P}_{\text{NG}}^{(\text{tlp})}(x, p) \mathcal{F}_{\text{NG}}(x, p) &= \sum_{i,j} (-1)^{i+j} \frac{1}{2\pi \mathcal{P}_{\text{det}}} \frac{1-\lambda^2}{1-\lambda^2 \gamma_i \gamma_j} \\ &\times \exp \left[-\mathcal{K}_{ij} \left\{ \left(x - \frac{\alpha_0^{(r)}}{\sqrt{2}} \right)^2 + \left(p - \frac{\alpha_0^{(i)}}{\sqrt{2}} \right)^2 \right\} \right], \end{aligned} \quad (\text{B3})$$

where

$$\mathcal{K}_{ij} = \frac{1-\lambda T - \lambda^2 \gamma_i \gamma_j - \frac{\lambda^2 T}{2} (\gamma_i + \gamma_j)}{1-\lambda^2 \gamma_i \gamma_j} \quad (\text{B4})$$

and $\alpha_0 \equiv \alpha_0^{(r)} + i\alpha_0^{(i)}$.

By integrating Eq. (B3) with respect to x and p , we obtain the average fidelity,

$$\begin{aligned} \bar{\mathcal{F}}_{\text{NG}}(\lambda) &= \sum_{i,j} (-1)^{i+j} \frac{1}{2\mathcal{P}_{\text{det}}} \frac{1-\lambda^2}{1-\lambda T - \lambda^2 \gamma_i \gamma_j - \frac{\lambda^2 T}{2} (\gamma_i + \gamma_j)} \\ &\equiv \sum_{i,j} (-1)^{i+j} \mathcal{F}_{ij}(\lambda). \end{aligned} \quad (\text{B5})$$

For the mutual information of dense coding, we calculate the homodyne probability distribution,

$$\begin{aligned} \mathcal{P}_{\text{NG}}^{(\text{HD})}(x, p|x_s, p_s) &= {}_{\text{AB}} \langle \Pi(x, p) | \hat{U}_{\text{A}}(x_s, p_s) \hat{\rho}_{\text{NG}} \hat{U}_{\text{A}}^\dagger(x_s, p_s) | \Pi(x, p) \rangle_{\text{AB}} \\ &= \frac{1}{2\pi \mathcal{P}_{\text{det}}} \frac{1-\lambda^2}{(1-\lambda T)^2 - \lambda^2 \gamma_i \gamma_j} \\ &\times \exp \left[-\frac{1-\lambda^2(T+\gamma_i)(T+\gamma_j)}{(1-\lambda T)^2 - \lambda^2 \gamma_i \gamma_j} |\xi'|^2 \right] \\ &\equiv \sum_{i,j} (-1)^{i+j} \mathcal{P}_{ij}(x, p|x_s, p_s), \end{aligned} \quad (\text{B6})$$

where ξ_s and ξ' are given in Eq. (A10).

With (B6), the component of channel matrix can be calculated. For example,

$$\begin{aligned}
& \mathcal{P}_{\text{NG}}^{(\text{ch})}(b_{00}|a_{00}) \\
&= \int_0^\infty dx \int_0^\infty dp \mathcal{P}_{\text{NG}}^{(\text{ch})}(x, p|\sqrt{2}\beta, \sqrt{2}\beta) \\
&= \sum_{i,j} \frac{(-1)^{i+j}}{4\mathcal{P}_{\text{det}}} \frac{1-\lambda^2}{1-\lambda^2(T+\gamma_i)(T+\gamma_j)} \\
&\quad \times \left[1 + \text{erf} \left(\sqrt{\frac{1-\lambda^2(T+\gamma_i)(T+\gamma_j)}{(1-\lambda T)^2 - \lambda^2\gamma_i\gamma_j}} \beta \right) \right]^2 \\
&\equiv \sum_{i,j} (-1)^{i+j} \mathcal{C}_{ij} [1 + \text{erf}(\Omega_{ij}\beta)]^2. \tag{B7}
\end{aligned}$$

Other components can be derived similarly. With these results, we can obtain the mutual information (57).

-
- [1] M. A. Nielsen and I. L. Chuang, *Quantum Computation and Quantum Information* (Cambridge University Press, Cambridge, 2000).
- [2] S. L. Braunstein and A. K. Pati, *Quantum Information with Continuous Variables* (Kluwer Academic Publishers, Dordrecht, 2003).
- [3] S. L. Braunstein and H. J. Kimble, Phys. Rev. Lett. **80**, 869 (1998); L. Vaidman, Phys. Rev. A **49**, 1473 (1994).
- [4] A. Furusawa, J. L. Sørensen, S. L. Braunstein, C. A. Fuchs, H. J. Kimble, and E. S. Polzik, Science **282**, 706 (1998).
- [5] T. C. Zhang, K. W. Goh, C. W. Chou, P. Lodahl, and H. J. Kimble, Phys. Rev. A **67**, 033802 (2003).
- [6] W. P. Bowen, N. Treps, B. C. Buchler, R. Schnabel, T. C. Ralph, Hans-A. Bachor, T. Symul, and P. K. Lam, *ibid* **67**, 032302 (2003).
- [7] M. Ban, J. Opt. B: Quantum Semiclass Opt. **1**, L9 (1999); S. L. Braunstein and H. J. Kimble, Phys. Rev. A **61**, 042302 (2000).
- [8] X. Li, Q. Pan, J. Jing, J. Zhang, C. Xie, and K. Peng, Phys. Rev. Lett. **88**, 047904 (2002).
- [9] J. Mizuno, K. Wakui, A. Furusawa, and M. Sasaki, Phys. Rev. A **71**, 012304 (2005).
- [10] X. Jia, X. Su, Q. Pan, J. Gao, C. Xie, and K. Peng, Phys. Rev. Lett. **93**, 250503 (2004).
- [11] N. Takei, H. Yonezawa, T. Aoki, and A. Furusawa, Phys. Rev. Lett. **94**, 220502 (2005).
- [12] J. Eisert, S. Scheel, and M. B. Plenio, Phys. Rev. Lett. **89**, 137903 (2002).
- [13] J. Fiurášek, Phys. Rev. Lett. **89**, 137904 (2002).
- [14] G. Giedke and J. I. Cirac, Phys. Rev. A **66**, 032316 (2002).
- [15] D. Gottesman, A. Kitaev, and J. Preskill, Phys. Rev. A **64**, 012310 (2001).
- [16] K. Nemoto and W. J. Munro, Phys. Rev. Lett. **93**, 250502 (2004).
- [17] T. Opatrný, G. Kurizki, and D.-G. Welsch, Phys. Rev. A **61**, 032302 (2000).
- [18] P. T. Cochrane, T. C. Ralph, and G. J. Milburn, Phys. Rev. A **65**, 062306 (2002).
- [19] D. E. Browne, J. Eisert, S. Scheel, and M. B. Plenio, Phys. Rev. A **67**, 062320 (2003).
- [20] S. Olivares, M. G. A. Paris, and R. Bonifacio, Phys. Rev. A **67**, 032314 (2003).
- [21] H. Nha and H. J. Carmichael, Phys. Rev. Lett. **93**, 020401 (2004).
- [22] R. Garcia-Patrón, J. Fiurášek, N. J. Cerf, J. Wenger, R. Tualle-Brouri, and Ph. Grangier, Phys. Rev. Lett. **93**, 130409 (2004); R. Garcia-Patrón, J. Fiurášek, and N. J. Cerf, Phys. Rev. A **71**, 022105 (2005).
- [23] S. Olivares and M. G. A. Paris, Phys. Rev. A **70**, 032112 (2004).
- [24] A. Kitagawa, M. Takeoka, K. Wakui, and M. Sasaki, Phys. Rev. A **72**, (2005).
- [25] G. Vidal, J. Mod. Opt. **47**, 355 (2000).
- [26] C. H. Bennett, D. P. DiVincenzo, J. A. Smolin, and W. K. Wootters, Phys. Rev. A **54**, 3824 (1996).
- [27] W. K. Wootters, Phys. Rev. Lett. **80**, 2245 (1998).
- [28] P. M. Hayden, M. Horodecki, and B. M. Terhal, J. Phys. A: Math. Gen. **34**, 6891 (2001).
- [29] V. Vedral and M. B. Plenio, Phys. Rev. A **57**, 1619 (1998).
- [30] G. Vidal and R. F. Werner, Phys. Rev. A **65**, 032314 (2002).
- [31] A. Peres, Phys. Rev. Lett. **77**, 1413 (1996).
- [32] M. Horodecki, P. Horodecki, and R. Horodecki, Phys. Rev. Lett. **89**, 2014 (2000).
- [33] M. B. Plenio and S. Virmani, arXiv:quant-ph/0504163.
- [34] M. B. Plenio, Phys. Rev. Lett. **95**, 090503 (2005).
- [35] J. Eisert, Ph.D. thesis, University of Potsdam, 2001.
- [36] G. Adesso and F. Illuminati, Phys. Rev. A **72**, 032334 (2005).
- [37] J. Eisert and M. B. Plenio, J. Mod. Opt. **46**, 145 (1999).